DOI: 10.1002/ejic.200700402

Organometallic and Classical Coordination Sites in Highly Preorganized Pyrazolate-Based Hybrid Systems: The Mn/Ni Case

Huaxin Zhang,[a] Sebastian Dechert,[a] Michael Linseis,[b] Rainer F. Winter,[b] and Franc Meyer*[a]

Keywords: Bridging ligands / Cyclopentadienyl ligands / Manganese / Nickel / Heterometallic complexes

A series of unsymmetric heterodinuclear Mn/Ni complexes is reported in which an organometallic $CpMn(CO)_2$ fragment and a classical Werner-type nickel(II) subunit are arranged in close proximity by means of a bridging pyrazolate. The two metalloligand scaffolds (**1** and **2**) employed differ in the chelate size of the tripodal tetradentate $\{N_4\}$ binding site for nickel. Molecular structures have been determined for ($\mathbf{1}_{-H}$)-Ni(NO_3) (**3**), ($\mathbf{2}_{-H}$)Ni(NO_3) (**4**), and ($\mathbf{2}_{-H}$)Ni(OAc) (**5**). Comparison with the molecular structures of the related Mn/Mn, Mn/Co, and Mn/Zn systems confirms that structural flexibility is greater for the complexes based on ligand **2** due to the longer chelate arms. According to IR and UV/Vis spectroelectrochemistry, oxidation of the heterobimetallic systems is highly localized at the organometallic manganese site. Structural and spectroscopic features as well as trends for the redox potentials of the Mn^I/Mn^{II} couple suggest that ligand variations at the nickel(II) Werner-type subunit exert only a small influence on the properties of the organometallic part. In contrast, reduction occurs at the nickel site and is strongly dependent on the anion present. The effects at the organometallic $CpMn(CO)_2$ subunit upon reduction of the proximate nickel ion are most pronounced for **5**.

Introduction

The pyrazolate heterocycle is a well established and useful bridging unit in bimetallic complexes.[1] Further preorganization of the two metal ions as well as modulation of their structural and electronic properties can be achieved by attaching chelating side arms to the 3- and 5-positions of the heterocycle.[2,3] The majority of such pyrazolate-derived dinucleating ligand scaffolds are symmetric, which means that these scaffolds provide two identical coordination pockets and favor the formation of homobimetallic complexes. Unsymmetrical pyrazolate ligands that allow the targeted assembly of heterobimetallic complexes, despite the intriguing metal ion cooperativity that can be expected for those systems,[4] are relatively scarce due to their more laborious synthesis.[5] An interesting situation with respect to the mutual effects of the proximate metal ions arises when the distinction between the two binding sites becomes very pronounced, such as in hybrid systems that contain an organometallic subunit next to a classical Werner-type subunit.

We have recently reported a series of unsymmetrical homo- and heterobimetallic complexes of type **A** that formally combine an organometallic $CpMn(CO)_2$ fragment **B** and a classical subunit of type **C** (Scheme 1).[6–8] The latter is reminiscent of the tripodal tetradentate tris(pyridylmethyl)amine systems that are well established in mononuclear coordination chemistry.[9] Manganese(II), cobalt(II), or zinc(II) ions with different co-ligands X can be accommodated in the Werner-type compartment of complexes **A**, with only subtle changes of the spectroscopic and redox properties of the organometallic site.[6–8] It appears that the two metal ions in these complexes are electronically quite independent. In contrast, strong electronic coupling was observed in the symmetric dimanganese complex **D**, which was shown to undergo two sequential metal-centered one-electron oxidations with fast intramolecular thermal electron transfer ($k_{ET} \approx 2.6 \times 10^{10}\ s^{-1}$ at 298 K) in the mixed-valent Mn^IMn^{II} species, which has a formal low-spin d^5d^6 electronic configuration.[10] The coincidence of the π plane of the heterocycle with the mirror plane of the $Mn(CO)_2$ moiety in **D** is an ideal arrangement for Mn-pyrazolate π-interactions and hence for electronic communication between the two Mn centers.[10–12]

In the present work we have now investigated a series of new heterobimetallic complexes of type **A** with nickel(II) in the tripodal tetradentate $\{N_4\}$ coordination site and different counteranions Y. A large separation of the metal-centered redox potentials was anticipated for this particular combination since oxidation of the manganese ion might

[a] Institut für Anorganische Chemie, Georg-August-Universität Göttingen
Tammanstraße 4, 37077 Göttingen, Germany
Fax: +49-551-393063
E-mail: franc.meyer@chemie.uni-goettingen.de
[b] Institut für Anorganische Chemie, Universität Regensburg
Universitätsstraße 31, 93040 Regensburg, Germany
Supporting information for this article is available on the WWW under http://www.eurjic.org or from the author.

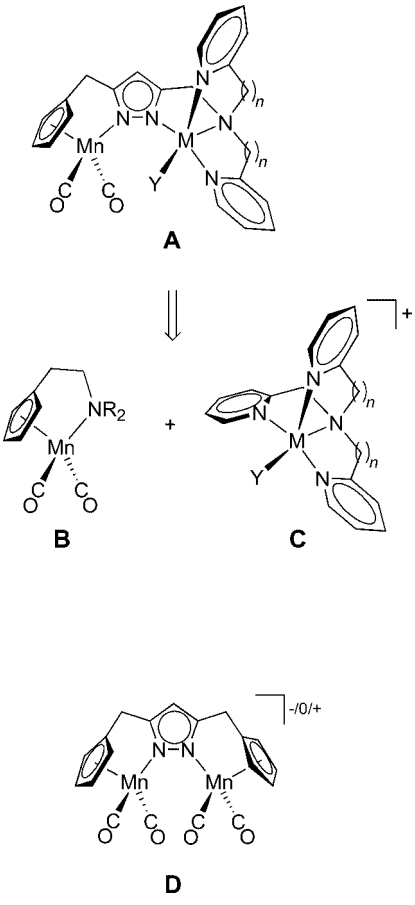

Scheme 1.

occur easily while nickel(I) or nickel(III) should be much harder to access. It therefore appeared interesting to probe whether one-electron redox processes would be strictly confined to one site and to what extent a mutual influence of the adjacent metal ions might be discernible for the Mn/Ni case.

Results and Discussion

Synthesis and Structural Characterization of the Complexes

Cymantrene derivatives **1** and **2** are the basic scaffolds for this particular class of heterobimetallic complexes (Scheme 2). They were prepared in several steps from simple pyrazole derivatives as reported previously,[6] with different lengths of the pyridylalkyl side-arms appended to the pyrazole heterocycle. The latter variation allows us to probe the effect of small changes of the Werner-type $\{N_4\}$ binding pockets on the properties of the bimetallic array. Photolysis of **1** or **2** with a high pressure mercury lamp in a quartz tube at –40 °C leads to CO release and intramolecular coordination of the pyrazole nitrogen atom to manganese, and subsequent deprotonation with one equivalent of KO*t*Bu followed by addition of the appropriate nickel salt [$Ni(NO_3)_2 \cdot 6H_2O$ or $Ni(OAc)_2 \cdot 4H_2O$] fills the $\{N_4\}$ donor compartment. This synthetic sequence is best carried out as a one-pot reaction.

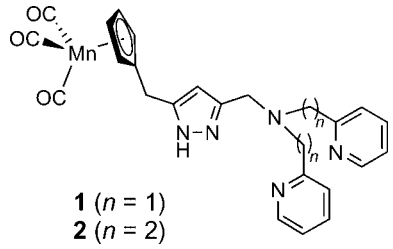

Scheme 2.

Single crystals of **3**·dmf, **4**, and **5** were obtained by slow diffusion of Et_2O into dmf solutions of the products (Scheme 3), and details of the constitution of all three complexes were elucidated by X-ray crystallography. The molecular structures are depicted in Figures 1, 2, and 3, together with selected interatomic distances and bond angles.

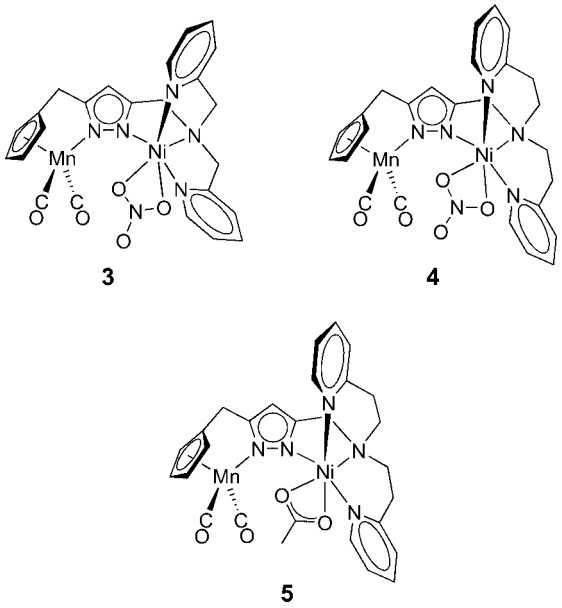

Scheme 3. Heterobimetallic Mn/Ni complexes.

The pyrazolate bridges the two metal ions in all three complexes **3**–**5** and the nickel(II) is hosted in the classical $\{N_4\}$ coordination site, as anticipated. Only complex **3** features crystallographically imposed mirror symmetry. Sixfold coordination of the nickel ion is completed by (slightly asymmetric) bidentate coordination of either a nitrate (**3**, **4**) or acetate anion (**5**), which results in a strongly distorted octahedral environment of the metal center. The metal–metal separation depends strongly on the length of the ligand side-arms. Thus, a larger Mn···Ni distance of around 4.50 Å is induced by the longer chelate arms in **4** and **5** whereas a distinctly shorter distance of 4.25 Å is observed for **3**. This variation is accompanied by different chelate arrangements of the Werner-type site: in the case of the shorter side-arms (**3**) the pyridyl nitrogens are located *trans* to each other and a nitrate oxygen is *trans* to the pyrazolate

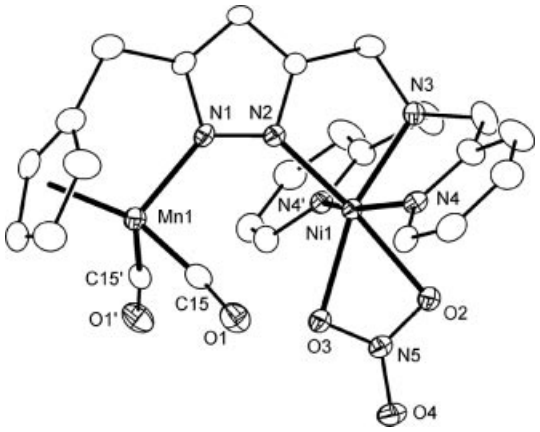

Figure 1. ORTEP plot (30% probability thermal ellipsoids) of the molecular structure of **3**. All hydrogen atoms have been omitted for the sake of clarity. Selected bond distances [Å] and angles [°] (Cg1 defines the centroid of the Cp ring atoms): Mn1–Cg1 1.771(3), Mn1–N1 2.017(4), Mn1–C15 1.764(4), Mn1···Ni1 4.247(1), Ni1–O2 2.192(4), Ni1–O3 2.093(4), Ni1–N2 2.008(4), Ni1–N3 2.090(4), Ni1–N4 2.064(3), O1–C15 1.165(5); Cg1–Mn1–N1 111.9(2), Cg1–Mn1–C15 124.0(2), C15–Mn(1)–C15′ 91.8(3), C15–Mn1–N1 100.1(2), O1–C15–Mn1 174.1(3), N2–Ni1–N3 84.5(2), N2–Ni1–N4 94.5(1), N2–Ni1–O2 174.1(2), N2–Ni1–O3 113.3(2), N3–Ni1–N4 82.1(1), N3–Ni1–O2 101.5(2), N3–Ni1–O3 162.2(2), N4–Ni1–N4′ 160.9(2), N4–Ni1–O2 86.4(1), N4–Ni1–O3 95.9(1), O2–Ni1–O3 60.8(1). Symmetry transformation used to generate equivalent atoms: (′) *x*, 3/2 – *y*, *z*.

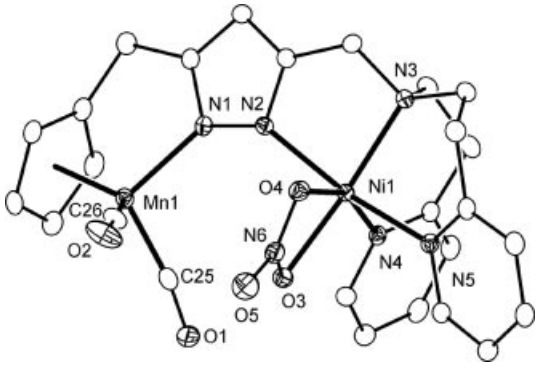

Figure 2. ORTEP plot (30% probability thermal ellipsoids) of the molecular structure of **4**. All hydrogen atoms have been omitted for the sake of clarity. Selected bond distances [Å] and angles [°] (Cg1 defines the centroid of the Cp ring atoms): Mn1–Cg1 1.773(1), Mn1–N1 2.050(2), Mn1–C25 1.760(3), Mn1–C26 1.766(3), Mn1···Ni1 4.5091(5), Ni1–O3 2.109(2), Ni1–O4 2.208(2), Ni1–N2 2.100(2), Ni1–N3 2.110(2), Ni1–N4 2.058(2), Ni1–N5 2.122(2), O1–C25 1.171(3), O2–C26 1.167(3); Cg1–Mn1–N1 112.8(1), Cg1–Mn1–C25 124.0(1), Cg1–Mn1–C26 123.7(1), C25–Mn(1)–C26 90.3(1), C25–Mn1–N1 104.9(1), C26–Mn1–N1 95.9(1), O1–C25–Mn1 170.9(2), O2–C26–Mn1 174.9(2), N2–Ni1–N3 81.9(1), N2–Ni1–N4 100.9(1), N2–Ni1–N5 166.9(1), N2–Ni1–O3 98.1(1), N2–Ni1–O4 88.6(1), N3–Ni1–N4 96.6(1), N3–Ni1–N5 90.8(1), N3–Ni1–O3 165.3(1), N3–Ni1–O4 105.3(1), N4–Ni1–N5 90.7(1), N4–Ni1–O3 97.9(1), N4–Ni1–O4 157.3(1), N5–Ni1–O3 86.1(1), N5–Ni1–O4 82.7(1), O3–Ni1–O4 60.1(1).

nitrogen, while for the longer side-arms (**4**, **5**) the pyrazolate is found *trans* to a pyridine nitrogen. Similar features and differences of the Mn···M separation of approximately 0.3 Å have been found for related Mn/Zn and Mn/Co com-

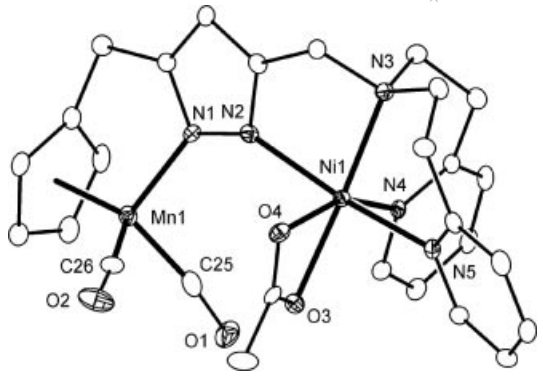

Figure 3. ORTEP plot (30% probability thermal ellipsoids) of the molecular structure of **5**. All hydrogen atoms have been omitted for the sake of clarity. Selected bond distances [Å] and angles [°] [Cg(1) defines the centroid of the Cp ring atoms]: Mn1–Cg1 1.773(2), Mn1–N1 2.045(3), Mn1–C25 1.751(5), Mn1–C26 1.759(5), Mn1···Ni1 4.507(1), Ni1–O3 2.072(3), Ni1–O4 2.193(3), Ni1–N2 2.118(3), Ni1–N3 2.114(4), Ni1–N4 2.075(3), Ni1–N5 2.143(3), O1–C25 1.184(5), O2–C26 1.174(5); Cg1–Mn1–N1 112.7(1), Cg1–Mn1–C25 123.8(2), Cg1–Mn1–C26 123.9(2), C25–Mn(1)–C26 90.3(2), C25–Mn1–N1 104.5(2), C26–Mn1–N1 96.5(2), O1–C25–Mn1 171.2(4), O2–C26–Mn1 174.3(5), N2–Ni1–N3 81.5(1), N2–Ni1–N4 101.0(1), N2–Ni1–N5 166.0(1), N2–Ni1–O3 100.2(1), N2–Ni1–O4 89.0(1), N3–Ni1–N4 95.9(1), N3–Ni1–N5 89.9(1), N3–Ni1–O3 166.6(1), N3–Ni1–O4 105.0(1), N4–Ni1–N5 90.8(1), N4–Ni1–O3 96.8(1), N4–Ni1–O4 158.0(1), N5–Ni1–O3 85.7(1), N5–Ni1–O4 82.5(1), O3–Ni1–O4 61.9(1).

plexes with the same pyrazole-based ligands.[6,8] The binding mode of the acetate or nitrate co-ligand (chelating, semi-chelating, or monodentate) depends on the radii and the particular stereoelectronic preferences of the metal ion in the $\{N_4\}$ binding pocket.

The Ni–O/N bond lengths of **3**–**5** lie within the range usually reported for octahedral nickel(II) complexes with a comparable N_4O_2 coordination sphere.[13] In particular, embedding of the nickel ion in the $\{N_4\}$ pocket is reminiscent of the situation found for a mononuclear nickel(II) acetate complex of type **C** with the tripodal tetradentate tris(pyridylmethyl)amine (TPA) ligand **E**.[14] This is in line with the description of complexes **3**–**5** as hybrids of an organometallic type **B** and a classical type **C** subunit. In the case of **E**, however, the acetate co-ligand is only monodentate and the remaining coordination site is occupied by a water molecule.

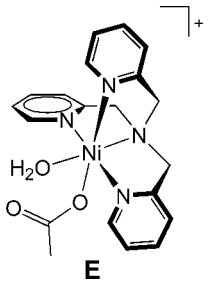

E

A comparison of the Mn–Cg (Cg defines the centroid of the ring atoms of the cyclopentadienido-anion), Mn–CO, Mn–N, and C≡O bond lengths of **3**–**5** and related Mn/Zn,

Table 1. Comparison of selected bond lengths [Å] and angles [°].

	Mn only[6]	Mn···Mn[7]	Mn···Co[8]	Mn···Zn[6]	Mn···Ni
Mn–Cg	1.77	1.76–1.77	1.76–1.77	1.77	1.77
Mn–N	2.01–2.02	2.01–2.03	2.01–2.05	1.99–2.03	2.02–2.05
Mn–CO	1.77–1.78	1.76–1.78	1.75–1.77	1.76–1.77	1.75–1.77
C≡O	1.16–1.17	1.16–1.17	1.17–1.20	1.16–1.19	1.17–1.18
Cg–Mn–N	111.2	111.6–112.7	112.1–112.5	110.8–112.5	111.9–112.8
Cg–Mn–CO	123.9–127.2	121.2–126.0	121.7–125.0	122.4–128.3	123.7–124.0
CO–Mn–CO	89.4–91.4	91.4–92.8	93.4–93.8	90.3–93.2	90.3–91.8
CO–Mn–N	96.0–102.2	94.8–102.7	99.5–104.1	94.6–101.4	95.9–104.9

Mn/Co, and Mn/Mn complexes, as well as complexes where the $\{N_4\}$ site is unoccupied, reveals that the choice of metal in the classical Werner-type site seems to have only a small influence on the bonding parameters of the organometallic $CpMn(CO)_2$ site (Table 1). Only the CO–Mn–N angles appear to be somewhat flexible and span a range from 94.8° to 104.1° (Table 1).

In order to visualize the extent of preorganization and the flexibility of the dimetallic arrangement based on **1** and **2**, a superposition of the pyrazolate-bridged cores of all Mn/Mn, Mn/Co, Mn/Ni, and Mn/Zn dinuclear complexes with either short or long chelate arms is shown in Figure 4. Structural variations should reflect the conformational freedom of the pyrazolate-centered dimetallic array, with the metal ions swinging above and below the heterocyclic plane. It seems that the range of displacements out of the plane of the pyrazolate heterocycle that is accessible to the two metal ions is greater in the case of the longer (and more flexible) side-arms at the $\{N_4\}$ compartment. The maximum angle between the pyrazolate plane and the N1–Mn bond is 11.1° for systems derived from **1** and 22.5° for systems derived from **2**; the maximum angle between the pyrazolate plane and the N2–M bond is 14.5° for systems derived from **1** and 17.9° for systems derived from **2**.

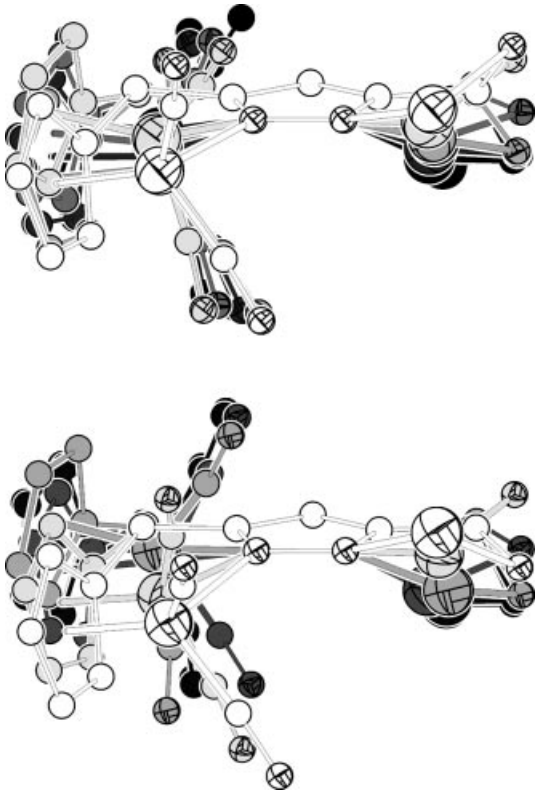

Figure 4. Overlay of the pyrazolate-bridged heterobimetallic arrangements for the series of Mn/Mn, Mn/Co, Mn/Ni, and Mn/Zn complexes based on **1** (short chelate arms; top) or **2** (long chelate arms; bottom). The appended chelate arms and the co-ligands at the Werner-type site have been omitted for clarity.

Spectroscopic and Electrochemical Trends

All Mn/Ni complexes show two strong IR bands of similar relative intensities for the $\nu_{as}(CO)$ and $\nu_s(CO)$ vibrations of the $\{Mn(CO)_2\}$ fragment at around 1900 and 1825 cm^{-1}, respectively (Table 2). Neither the chelate ring size of the $\{N_4\}$ ligand compartment (**3** vs. **4**) nor the co-ligand at nickel (nitrate in **4** vs. acetate in **5**) seem to have any considerable effect on the energies of the CO stretches. Complex **5** features strong bands at 1550 and 1447 cm^{-1} that are absent in the spectrum of **4** and are thus assigned to the acetate ligand. The small difference between $\nu_{as}(COO)$ and $\nu_s(COO)$ is in accordance with bidentate acetate coordination.[15]

Table 2. IR absorptions [cm^{-1}] in the CO stretching range.

	dce solution[a]	KBr pellets
3	1902, 1825	1902, 1822
3$^+$	2029, 1949	
4	1906, 1829	1906, 1822
4$^+$	2029, 1950	
5	1904, 1827	1890, 1823
5$^+$	2029, 1950	

[a] dce = 1,2-dichloroethane.

Cyclic voltammograms in MeCN (**3**) or dmf (**4**, **5**) solution feature a reversible redox wave in the range $E_{1/2}$ = –0.50 to –0.66 V and an irreversible reduction at much lower potential (Table 3).[16] The cyclic voltammograms of **4** and **5** depicted in Figures 5 and 6, respectively, show that variations in the co-ligand at nickel (nitrate in **4** vs. acetate in **5**) barely influence the first redox process at around –0.6 V but have a pronounced effect on the reduction at lower potential. The former is thus assigned to the Mn^I/Mn^{II} couple while the latter process likely corresponds to the $Ni^{II} \rightarrow Ni^I$ reduction. Potentials for the Mn^I/Mn^{II} interconversions of $[CpMn(CO)_2L]$ complexes are known to

vary over a potential range of more than 2 V, depending of the nature of the ligand L.[11,12,17] The rather low oxidation potentials of **3**–**5** indicate significant stabilization of the Mn^{II} state by the anionic pyrazolate ligand and reflect the high nucleophilicity of the nitrogen heterocycle in these heterobimetallic species.[17] Small influences of the ligand chelate ring size (**3** vs. **4**) or of the co-ligand at nickel (**4** vs. **5**) on the Mn^{I}/Mn^{II} redox potential suggest a certain degree of electronic communication between the proximate metal ions. For example, the oxidation wave of the nitrate complex with shorter chelate arms at nickel (**3**) is shifted anodically by 60 mV with respect to the congener with longer chelate arms (**4**), and the more electron-donating acetate at nickel facilitates oxidation of the manganese site by 100 mV (**5** vs. **4**). These trends are in good agreement with findings for the related Mn/Mn, Mn/Co, and Mn/Zn systems.[6–8]

Table 3. Formal potentials for the Mn^{I}/Mn^{II} couple in MeCN/0.1 M nBu$_4$NClO$_4$ (**3**) or dmf/0.1 M nBu$_4$NPF$_6$ (**4**, **5**).[16]

Complex	$E_{1/2}(Mn^{I}Ni^{II}/Mn^{II}Ni^{II})$	$E^{p}_{red}(Mn^{I}Ni^{II}/Mn^{I}Ni^{I})$
3	–0.50	–1.70[a]
4	–0.56	–1.83[a]
5	–0.66	–2.72[a]

[a] Peak potentials for irreversible reduction process at 100 mV s^{-1}.

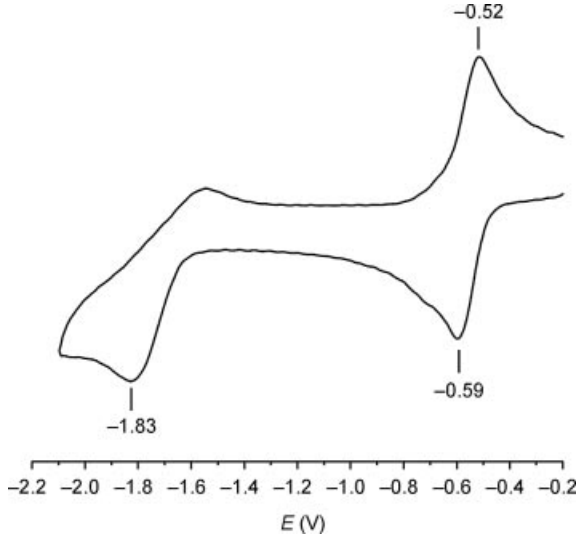

Figure 5. Cyclic voltammogram of **4** recorded with a platinum electrode in dmf containing approximately 0.1 M nBu$_4$NPF$_6$; scan speed: 100 mV s^{-1}; potentials are given in volts vs. the Fc/Fc$^+$ couple.

IR and UV/Vis spectroelectrochemistry have proven valuable for establishing the site of redox processes in such heterobimetallic complexes and to characterize the resulting species. Oxidation of the Mn/Ni systems **3**–**5** in 1,2-dichloroethane (dce) was thus followed by IR and UV/Vis spectroscopy in an OTTLE cell (Figures 7 and 8, and Figures S1–S4 in the Supporting Information). The intensity of the pair of CO stretching vibrations at around 1905 and 1825 cm^{-1} decreases at the expense of two new bands at around 2030 and 1950 cm^{-1} upon gradual electrolysis, thus confirming the structural integrity of the $CpMn(CO)_2$ frag-

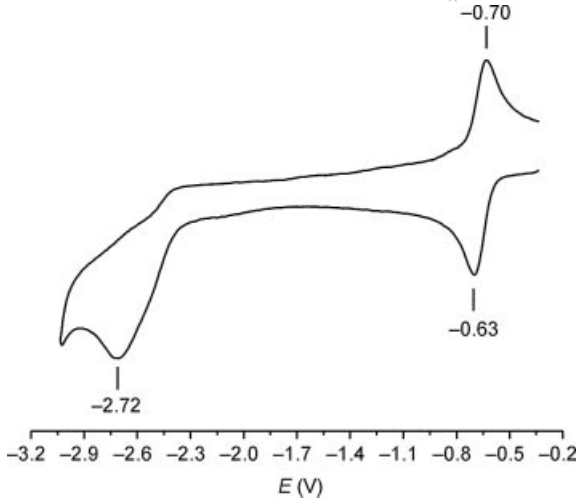

Figure 6. Cyclic voltammogram of **5** recorded with a platinum electrode in dmf containing approximately 0.1 M nBu$_4$NPF$_6$; scan speed: 100 mV s^{-1}; potentials are given in volts vs. the Fc/Fc$^+$ couple.

ment upon generation of the oxidized species **3**$^+$–**5**$^+$. The slightly lower intensity of the new bands is in agreement with our expectations since spectral intensities in M–CO moieties usually decrease with increasing oxidation state.[18] The shift of about 125 cm^{-1} to higher frequencies is very similar to the shift observed in the corresponding Mn/Zn, Mn/Co and Mn/Mn complexes.[6–8] It is typical for a one-unit increase in the oxidation state of the metal ion and reflects the diminished backbonding ability in the oxidized $CpMn^{II}(CO)_2$ subunit. This confirms that the anodic process in the present Mn/Ni systems is fully localized at the organometallic site, which means that nickel remains in the +II oxidation state. The presence of several isosbestic points confirms clean conversion between the $Mn^{I}Ni^{II}$ and Mn^{II}-Ni^{II} species. However, the original spectra of the starting materials **3**–**5** are not fully restored upon re-reduction. Furthermore, the intensities of the CO stretching vibrations

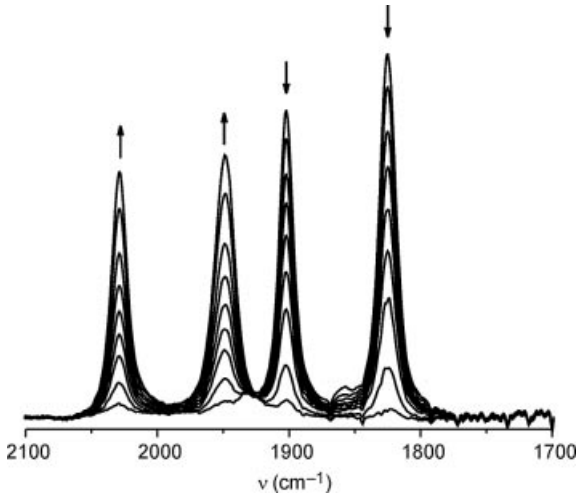

Figure 7. IR spectroscopic changes during the gradual oxidation of **3** in dce/nBu$_4$PF$_6$ solution in an OTTLE cell.

are somewhat lower than their original values, which suggests that the oxidized complexes have only limited stabilities in solution. Accordingly, attempts to crystallize the $Mn^{II}Ni^{II}$ complexes after chemical oxidation have so far proved unsuccessful.

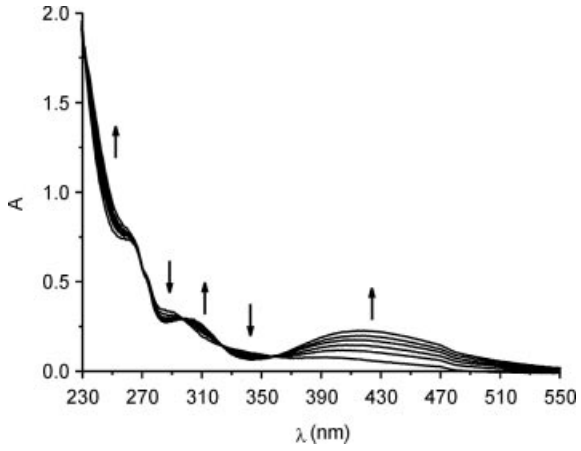

Figure 8. UV/Vis spectroscopic changes during the gradual oxidation of **3** in dce/nBu$_4$PF$_6$ solution in an OTTLE cell.

The oxidation of **3**–**5** is accompanied in UV/Vis spectroelectrochemistry by the appearance of a new band peaking in the range 395–421 nm (**3**: 415 nm; **4**: 396 nm; **5**: 421 nm, Figure 8 and S3, S4). The rise of a similar band at about 400 nm has also been observed upon oxidation of the corresponding Mn/Zn, Mn/Co and Mn/Mn systems[6–8] and can thus be safely assigned to the π(pyrazolate)→CpMn^{II}-(CO)$_2$ LMCT transition, which is obviously relatively insensitive to the identity of the metal ion within the adjacent Werner-type {N$_4$} compartment.

According to IR spectroelectrochemistry, reduction of **4** is also an almost reversible process. Shifts to lower energy in the CO stretching range are only minor (Figures 9 and 10; 1906/1829→1902/1827 cm^{-1} for **4**; 1906/1829→1896/1819 cm^{-1} for **5**), in accordance with the idea that reduction occurs within the nickel subunit. It is interesting to note, however, that the CO stretches are clearly more affected in **5**, where a noticeable shift of 10 cm^{-1} is observed compared to an almost negligible shift of about 3 cm^{-1} for **4**. Since **4** and **5** are derived from the same pyrazolate-based ligand scaffold, this distinction must stem solely from the different anion at nickel (nitrate vs. acetate). Re-oxidation of **5**$^-$ does not reproduce the original spectrum but gives rise to a new species with two IR bands that are shifted by 18 cm^{-1} to lower energy with respect to the CO absorptions of **5**. While the typical pattern of two CO stretches suggests that the integrity of the CpMn(CO)$_2$ subunit is retained, the chemical reaction that apparently follows upon electrochemical reduction may involve a ligand exchange at nickel or ligand fragmentation at the Werner-type site. The rather different behavior of **4** and **5** upon reduction is in accordance with the strongly different reduction potentials determined electrochemically for these two complexes (compare Figures 5 and 6).

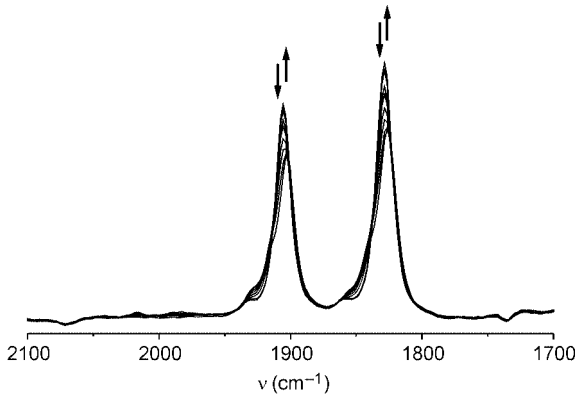

Figure 9. IR spectroscopic changes during the gradual reduction of **4** in dce/nBu$_4$PF$_6$ solution in an OTTLE cell.

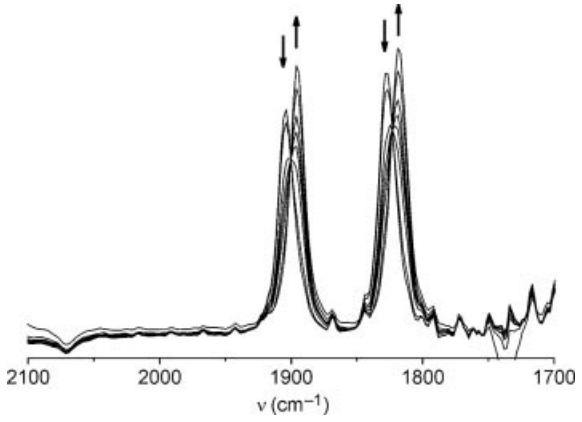

Figure 10. IR spectroscopic changes during the gradual reduction of **5** in dce/nBu$_4$PF$_6$ solution in an OTTLE cell.

Conclusions

The present set of Mn/Ni complexes complements a series of unique heterobimetallic systems in which an organometallic CpMn(CO)$_2$ fragment is bridged via a pyrazolate to a nearby metal ion (Mn^{2+}, Co^{2+}, Ni^{2+}, Zn^{2+}) that is nested in a classical Werner-type compartment with an {N$_4$} donor set. The pronounced asymmetry of the bimetallic array results in strong localization of redox events in those systems: oxidation occurs at relatively low potential and is strictly confined to the organometallic site, while reduction (in the case of Mn^{2+}, Co^{2+}, or Ni^{2+} as the second metal ion) appears to occur solely within the Werner-type subunit, with very little mutual interaction. Ligand variations at the {N$_4$} compartment (such as different lengths of the chelate arms or different co-ligands) exert only minor influences on the CpMn(CO)$_2$ fragment, but have a clear effect on the properties of the second metal ion, as expected. Further modifications of the Werner-type subunit, including donor sets other than the tripodal tetradentate {N$_4$} motif of the present complexes, should allow us to shift the redox potential of the second metal ion closer to that of the organometallic Mn site. It will be interesting to monitor the changes of intermetallic communication that might accompany such modifications and to probe the co-

operative redox transformation of substrates that bind to the second metal but exploit the strong reduction potential of the nearby organometallic site.

Experimental Section

General Procedures and Methods: Manipulations were carried out under an atmosphere of dry nitrogen by employing standard Schlenk techniques. Complexes **1** and **2** were prepared as reported previously.[6] Solvents were dried according to established procedures. All other chemicals were obtained from commercial sources and used as received. IR spectra were recorded for KBr pellets with a Digilab Excalibur. ESI mass spectra were measured with a Finnigan MAT LCQ spectrometer. Elemental analyses were performed by the analytical laboratory of the Institut für Anorganische Chemie der Universität Göttingen using a Heraeus CHN-O-RAPID instrument. Cyclic voltammetry was carried out with a Perkin–Elmer Model 263A potentiostat/galvanostat with glassy carbon working electrode and platinum reference and counter electrodes, in 0.1 M nBu$_4$NClO$_4$/CH$_3$CN or 0.1 M nBu$_4$NPF$_6$/dmf; ferrocene (the potential in dmf being 0.45 V against SCE)[19] was used as internal standard. Spectroelectrochemistry (IR and UV/Vis) was performed with a self-constructed OTTLE cell comprising a Pt-mesh working and counter electrode and a silver wire as pseudeo-reference electrode sandwiched in between the CaF_2 windows of a conventional liquid IR cell. The working electrode is positioned in the center of the spectrometer beam with all other parts of the cell made non-transparent to the incident beam by means of an absorbing tape.[20]

Synthesis of Complex 3: A solution of **1** (0.256 g, 0.52 mmol) in thf (200 mL) was irradiated with a high-pressure mercury lamp in a quartz tube at –40 °C. Within one hour the color of the solution had changed from light yellow to yellow. The solution was then warmed to room temperature and KOtBu (0.058 g, 0.52 mmol) and Ni(NO$_3$)$_2$·6H$_2$O (0.151 g, 0.52 mmol) were added. The reaction mixture was stirred overnight to produce a yellow precipitate, which was separated by filtration, washed with light petroleum ether, and dried under vacuum. Single crystals were obtained after several days by slow diffusion of diethyl ether into a concentrated dmf solution of the crude product. The crystals were separated by filtration, washed with diethyl ether, and dried under vacuum. Yield: 31 mg (9%). IR (KBr): $\tilde{\nu}$ = 2929 (w), 2869 (w), 1902 (vs), 1822 (vs), 1672 (m), 1605 (m), 1479 (m), 1384 (m), 1287 (m), 1157 (w), 1097 (w), 1056 (w), 1024 (w), 958 (w), 884 (w), 818 (w), 771 (m), 653 (w), 611 (w), 588 (w), 512 (w), 474 (w), 427 (w) cm^{-1}. $C_{27}H_{28}MnN_7NiO_6$ (660.2): calcd. C 49.12, H 4.27, N 14.85; found C 49.27, H 4.44, N 13.98.

Synthesis of Complex 4: A solution of **2** (0.230 g, 0.44 mmol) in thf (200 mL) was irradiated with a high pressure mercury lamp in a quartz tube at –40 °C. Within about one hour the color of the solution had changed from light yellow to yellow. The solution was then warmed to room temperature and KOtBu (0.049 g, 0.44 mmol) and Ni(NO$_3$)$_2$·6H$_2$O (0.128 g, 0.44 mmol) were added. The reaction mixture was stirred overnight to produce a yellow precipitate, which was separated by filtration, washed with light petroleum, and dried under vacuum. Single crystals were obtained after several days by slow diffusion of diethyl ether into a concentrated dmf solution of the crude product. The crystals were separated by filtration, washed with diethyl ether, and dried under vacuum. Yield: 40 mg (15%). IR (KBr): $\tilde{\nu}$ = 2963 (w), 2916 (w), 2864 (w), 1906 (vs), 1822 (vs), 1662 (w), 1607 (m), 1578 (w), 1487 (m), 1451 (m), 1387 (m), 1340 (w), 1276 (m), 1155 (w), 1105 (m), 1052 (w), 1022 (m), 950 (w), 807 (w), 765 (m), 656 (w), 591 (w), 528 (w), 474 (w), 432 (w) cm^{-1}. HR-MS (ESI+, MeCN): m/z calcd. for $C_{26}H_{25}MnN_6NiO_5$ [M]$^+$: 614.06149; found 614.06132. $C_{26}H_{25}MnN_6NiO_5$ (615.2): calcd. C 50.77, H 4.10, N 13.66; found C 49.50, H 4.27, N 13.62.

Synthesis of Complex 5: A solution of **2** (0.200 g, 0.38 mmol) in thf (200 mL) was irradiated with a high pressure mercury lamp in a quartz tube at –40 °C. Within about one hour the color of the solution had changed from light yellow to yellow. The solution was

Table 4. Crystal data and refinement details for **3**, **4**, and **5**.

	3·dmf	**4**	**5**
Formula	$C_{24}H_{21}MnN_6NiO_5$, C_3H_7NO	$C_{26}H_{25}MnN_6NiO_5$	$C_{28}H_{28}MnN_5NiO_4$
M_r	660.21	615.17	612.20
Crystal size [mm]	0.38 × 0.25 × 0.15	0.49 × 0.31 × 0.20	0.20 × 0.13 × 0.08
Crystal system	monoclinic	monoclinic	monoclinic
Space group	$P2_1/m$ (no. 11)	$P2_1/n$ (no. 14)	$P2_1/n$ (no. 14)
a [Å]	8.2387(6)	9.8289(6)	9.8625(8)
b [Å]	16.1559(8)	21.7710(15)	22.0007(18)
c [Å]	11.2310(7)	11.8129(7)	12.1508(11)
β [°]	107.879(5)	99.659(5)	101.311(7)
V [Å^3]	1422.69(15)	2491.9(3)	2585.3(4)
Z	2	4	4
$\rho_{calcd.}$ [g cm^{-3}]	1.541	1.640	1.573
F(000)	680	1264	1264
μ [mm^{-1}]	1.160	1.314	1.262
T_{max}/T_{min}	0.8422/0.6728	0.7909/0.6217	0.8754/0.6491
hkl range	±9, ±18, ±13	±11, –25 to 24, ±13	–11 to 10, ±25, ±14
θ range [°]	1.91–24.69	1.87–24.83	1.85–24.81
Measured reflections	23598	15798	13272
Unique reflections [R_{int}]	2516 [0.0641]	4270 [0.0405]	4434 [0.0993]
Observed reflections $I > 2\sigma(I)$	2159	3460	2844
Data/restraints/parameters	2516/2/210	4270/0/352	4434/0/353
Goodness-of-fit	1.066	1.002	1.005
$R1$ [$I > 2\sigma(I)$]	0.0498	0.0293	0.0492
$wR2$ (all data)	0.1480	0.0706	0.0669
Residual electron density [e Å^{-3}]	1.505/–0.538	0.313, –0.320	0.451/–0.401

then warmed to room temperature and KO*t*Bu (0.043 g, 0.38 mmol) and $Ni(CH_3COO)_2 \cdot 4H_2O$ (0.095 g, 0.38 mmol) were added. The reaction mixture was stirred overnight to produce a yellow precipitate, which was separated by filtration, washed with light petroleum, and dried under vacuum. Single crystals were obtained after several days by slow diffusion of diethyl ether into a concentrated dmf solution of the crude product. The crystals were separated by filtration, washed with diethyl ether, and dried under vacuum. Yield: 36 mg (16%). IR (KBr): $\tilde{\nu}$ = 2964 (w), 2917 (m), 2861 (w), 1890 (vs), 1823 (vs), 1666 (m), 1607 (m), 1550 (m), 1478 (m), 1447 (m), 1335 (m), 1259 (m), 1208 (w), 1148 (w), 1107 (m), 1052 (m), 1021 (m), 950 (w), 896 (w), 812 (m), 771 (m), 668 (w), 608 (w), 528 (w), 467 (w), 433 (w), 410 (w) cm^{-1}. HR-MS (ESI+, MeCN): *m*/*z* calcd. for $C_{28}H_{28}MnN_5NiO_4$ $[M]^+$: 611.08698; found 611.08634. $C_{28}H_{28}MnN_5NiO_4$ (612.2): calcd. C 54.93, H 4.61, N 11.44; found C 53.91, H 4.70, N 11.36.

X-ray Crystallography of Complexes 3–5: X-ray data were collected with a STOE IPDS II diffractometer (graphite-monochromated Mo-K_α radiation, λ = 0.71073 Å) using the ω-scans technique at –140 °C (Table 4). The structures were solved by direct methods and refined on F^2 using all reflections with SHELX-97.[21] The non-hydrogen atoms were refined anisotropically. Hydrogen atoms were placed in calculated positions and assigned an isotropic displacement parameter of 0.08 $Å^2$. Face-indexed absorption corrections were performed numerically with the program X-RED.[22] The geometrical aspects of the structures were analyzed with the PLATON program.[23] The dmf solvent molecule in **3**·dmf was found to be disordered about a center of inversion and was refined at half occupancy.

CCDC-638867 (for **3**·dmf), -638868 (for **4**), and -638869 (for **5**) contain the supplementary crystallographic data for this paper. These data can be obtained free of charge from The Cambridge Crystallographic Data Centre via www.ccdc.cam.ac.uk/data_request/cif.

Supporting Information (see also the footnote on the first page of this article): IR spectroscopic changes during gradual oxidation **4**→**4**$^+$ and **5**→**5**$^+$ in dce/nBu$_4$PF$_6$ solution in an OTTLE cell (Figures S1 and S2); UV/Vis spectroscopic changes during gradual oxidation **4**→**4**$^+$ and **5**→**5**$^+$ in dce/nBu$_4$PF$_6$ solution in an OTTLE cell (Figures S3 and S4).

Acknowledgments

Support by the Alexander von Humboldt foundation (research fellowship to H. Z.) is gratefully acknowledged. We thank J. Teichgräber for performing the CV measurements.

[1] a) S. Trofimenko, *Progr. Inorg. Chem.* **1986**, *34*, 115–210; b) G. La Monica, G. A. Ardizzoia, *Progr. Inorg. Chem.* **1997**, *46*, 151–238; c) R. Mukherjee, *Coord. Chem. Rev.* **2000**, *203*, 151–218.
[2] C. Incarvito, A. L. Rheingold, A. L. Gavrilova, C. J. Qin, B. Bosnich, *Inorg. Chem.* **2001**, *40*, 1386–1390.
[3] J. Klingele, S. Dechert, F. Meyer, *Coord. Chem. Rev.*, manuscript in preparation.
[4] a) D. E. Fenton, H. Okawa, *Chem. Ber./Recueil* **1997**, *130*, 433–442; b) D. E. Fenton, *Inorg. Chem. Commun.* **2002**, *5*, 537–547; c) R. Bosnich, *Inorg. Chem.* **1999**, *38*, 2554–2562; d) C. J. Qin, A. Gavrilova, B. Bosnich, *Pure Appl. Chem.* **2001**, *73*, 221–226; e) C. Belle, J.-L. Pierre, *Eur. J. Inorg. Chem.* **2003**, 4137–4146.
[5] a) M. Konrad, F. Meyer, K. Heinze, L. Zsolnai, *J. Chem. Soc. Dalton Trans.* **1998**, 199–205; b) M. Konrad, S. Wuthe, F. Meyer, E. Kaifer, *Eur. J. Inorg. Chem.* **2001**, 2233–2240.
[6] a) J. C. Röder, F. Meyer, E. Kaifer, *J. Organomet. Chem.* **2002**, *641*, 113–120; b) T. Sheng, S. Dechert, A. C. Stückl, F. Meyer, *Eur. J. Inorg. Chem.* **2005**, 1293–1302.
[7] T. Sheng, S. Dechert, I. Hyla-Kryspin, R. F. Winter, F. Meyer, *Inorg. Chem.* **2005**, *44*, 3863–3874.
[8] H. Zhang, S. Dechert, J. Maurer, M. Linseis, R. F. Winter, F. Meyer, *J. Organomet. Chem.* **2007**, *692*, 2956–2964.
[9] A. G. Blackman, *Polyhedron* **2005**, *24*, 1–39.
[10] a) J. C. Röder, F. Meyer, E. Kaifer, *Angew. Chem.* **2002**, *114*, 2414–2417; *Angew. Chem. Int. Ed.* **2002**, *41*, 2304–2306; b) J. C. Röder, F. Meyer, I. Hyla-Kryspin, R. F. Winter, E. Kaifer, *Chem. Eur. J.* **2003**, *9*, 2636–2648.
[11] K. G. Caulton, *Coord. Chem. Rev.* **1981**, *38*, 1–43.
[12] W. Kaim, R. Gross, *Comments Inorg. Chem.* **1988**, *7*, 269–285.
[13] F. Meyer, H. Kozlowski, in *Comprehensive Coordination Chemistry II* (Eds.: J. A. McCleverty, T. J. Meyer), Elsevier, Oxford, UK, **2004**, vol. 6, pp. 247–554.
[14] T. Nagataki, Y. Tachi, S. Itoh, *Chem. Commun.* **2006**, 4016–4018.
[15] a) G. B. Deacon, R. J. Phillips, *Coord. Chem. Rev.* **1980**, *33*, 227–250; b) V. Robert, G. Lemercier, *J. Am. Chem. Soc.* **2006**, *128*, 1183–1187.
[16] Values vs. the ferrocene/ferrocenium couple. $\Delta E_p = E_p^{ox} - E_p^{red}$ = 64 (for **3**), 88 (for **4**), or 65 mV (for **5**) with $\Delta E_p(Cp_2Fe/Cp_2Fe^+)$ = 60 (for **3**), 69 (for **4**), or 80 mV (for **5**) under the same experimental conditions.
[17] R. Gross, W. Kaim, *Angew. Chem.* **1985**, *97*, 869–870; *Angew. Chem. Int. Ed. Engl.* **1985**, *24*, 856–858; P. M. Zizelman, C. Amatore, K. Kochi, *J. Am. Chem. Soc.* **1984**, *106*, 3771–3784.
[18] a) J. P. Bullock, K. R. Mann, *Inorg. Chem.* **1989**, *28*, 4006–4011; b) D. T. Pierce, W. E. Geiger, *Inorg. Chem.* **1994**, *33*, 373–381.
[19] N. G. Connelly, W. E. Geiger, *Chem. Rev.* **1996**, *96*, 877–910.
[20] M. Kreijcik, M. Daniek, F. Hartl, *J. Electroanal. Chem.* **1991**, *317*, 179–187.
[21] G. M. Sheldrick, *SHELXL-97, Program for Crystal Structure Refinement*, University of Göttingen, Germany, **1997**; G. M. Sheldrick, *SHELXS-97, Program for Crystal Structure Solution*, University of Göttingen, Germany, **1997**.
[22] *X-RED*, STOE & CIE GmbH, Darmstadt, **2002**.
[23] A. L. Spek, *PLATON, A Multipurpose Crystallographic Tool*, Utrecht University, **2003**.

Received: April 12, 2007
Published Online: August 22, 2007

